APL Energy

REVIEW ARTICLE | JULY 07 2023

Halide double-perovskites: High efficient light emission and beyond

Daniela Marongiu ; Stefano Lai ; Fang Liu ; Angelica Simbula ; Francesco Quochi ; Michele Saba ; Andrea Mura ; Giovanni Bongiovanni

APL Energy 1, 021501 (2023)
https://doi.org/10.1063/5.0152473

AIP Publishing

APL Energy REVIEW pubs.aip.org/aip/ape

Halide double-perovskites: High efficient light emission and beyond

Cite as: APL Energy 1, 021501 (2023); doi: 10.1063/5.0152473
Submitted: 30 March 2023 • Accepted: 25 June 2023 •
Published Online: 7 July 2023

Daniela Marongiu,[1,a] Stefano Lai,[1] Fang Liu,[2] Angelica Simbula,[1] Francesco Quochi,[1] Michele Saba,[1] Andrea Mura,[1] and Giovanni Bongiovanni[1]

AFFILIATIONS

[1] Dipartimento di Fisica, Università degli Studi di Cagliari, Monserrato, CA 09042, Italy
[2] School of Environmental Science and Engineering, Frontiers Science Center for Transformative Molecules, Shanghai Jiao Tong University, Shanghai 200240, China

[a] **Author to whom correspondence should be addressed:** dmarongiu@dsf.unica.it

ABSTRACT

Lead-free halide double perovskites are stable and versatile materials for a wide range of applications, particularly for lighting, thanks to their very efficient emission of warm white light. Element substitution in halide double perovskite is recognized as a powerful method for tuning the emission wavelength and improve the efficiency. This review provides an overview on composition and recent progress in halide double perovskite with main focus on the synthesis and emission properties of chloride-based compounds.

I. INTRODUCTION

In recent years, inorganic chloride-based lead-free double perovskites (DPs) with formula $Cs_2M^+M^{3+}Cl_6$, more properly known as elpasolites, have emerged as single-component white light emitters for phosphors and LEDs.

The most prominent property of DPs is broadband, visible light emission with quantum yield approaching unity, a feature that, combined with outstanding stability, has motivated researchers to study in depth their properties and photophysics. Furthermore, the versatile perovskite structure allows to incorporate a variety of ions as substituting elements, resulting in the opportunity to control the absorption and emission processes. Both absorption and emission spectra of double perovskites are ideally suited for lighting purposes. The absorption is typical of large gap semiconductors and insulators, with a steep, direct bandgap in the blue or near UV spectral region so that most compounds are transparent across most or all the visible spectrum. On the other hand, emission is broadband and mostly in the visible spectrum. The corresponding color temperature spans from warm white (as low as 2500 K color temperature) to cold white (higher than 6000 K), with extremely high color rendering index values. DPs compare therefore very favorably with the current technology for white light emission, which is based on semiconductor compounds, such as InGaN, with yellow emitting YAG:Ce^{3+}; however, the resulting light typically lacks a red component thus generating a cool-white emission not ideal for indoor general lighting.[1]

Recent reviews describe the developments of DPs both in the form of colloidal nanocrystals and microcrystals, also insights from computational studies and thermodynamic stability are explored along with other emerging DP-inspired materials such as the so-called vacancy-ordered perovskite in the form of $Cs_2M^{4+}X_6$.[2–5] This review will explore the physical origin of the optical properties of double perovskites, specifically the Na/Ag and In-based, combining both experimental evidence and insights from computational studies. In particular, the discussion will highlight the roles of self-trapped excitons of parity forbidden optical transitions and of localized orbitals. Synthesis strategies and composition for the most studied double perovskites will be reviewed, including the partial substitution of M^+ or M^{3+} elements with a vast library of metal ions to tune optical properties.

Chloride-based microcrystalline DPs will be discussed explicitly, although most of the arguments are common to their colloidal nanocrystalline counterparts. A brief paragraph is also devoted to the only bromide-based stable compound $Cs_2AgBiBr_6$.

Finally, the prospects for applications will be discussed, including phosphors, light-emitting devices, and fast and nontoxic photodetectors for UV light and biomedical imaging.

II. CHLORIDE DOUBLE PEROVSKITE: $Cs_2M^+M^{3+}Cl_6$

A. Crystal structure

The general halide perovskite AMX_3 has a crystal structure characterized by the M^{2+} ions octahedrally coordinated in a 3D network of corner-sharing $[MX_6]$ octahedra and the A^+ ion in the sites among them [Fig. 1(a)].

The crystal symmetry of a general perovskite AMX_3 can be predicted by the Goldschmidt tolerance factor t, which depends on the size of cation (r_A), metal (r_M), and halide (r_X) radii[6]

$$t = \frac{r_A + r_X}{\sqrt{2}(r_M + r_X)}.$$

The octahedral structure is not rigid; instead, it can accommodate distortions that often improve lattice stability. The Goldschmidt tolerance factor is typically between 0.7 and 1.1 and measures the degree of distortion. The ideal perovskite structure has $t \approx 1$ and is cubic. When r_A is larger than the optimal value, then $t > 1$ and the structure becomes hexagonal with the M^{2+} ion moving away from the octahedral center. On the other hand, if r_A is too small, $0.75 < t < 1$, the MX_6 octahedra undergo a tilt, like in prototypical hybrid perovskite $MAPbI_3$ (methylammonium lead iodide, $CH_3NH_3PbI_3$), and the structure becomes orthorhombic.[7] The structure not only determines the stability but also defect formation energy and influences the electronic bands; therefore, many of the perovskite properties depend on the kind of lattice distortion with respect to the ideal cubic structure.

The M^{2+} cation can be replaced by a monovalent and a trivalent ion thus neutralizing the overall charge in the lattice and resulting in the elpasolite or ordered double perovskite $Cs_2M^+M^{3+}Cl_6$ [Fig. 1(b)]. The definition of the Goldschmidt tolerance factor t can be extended to double perovskites by using the arithmetic average of the two M-site radii as the radius of the metal cation r_M. The range of stability is found for $0.8 < t < 1$.[8] However, additional conditions exist limiting the size mismatch between the two metal cations, for example, the limit case for rather small size M^+ ions, such as lithium, where hexagonal symmetry is observed even if coupled with large size M^{3+} ions, such as lutetium, with $t = 0.978$.[9]

The crystal structure of halide DPs $Cs_2M^+M^{3+}Cl_6$ is face-centered cubic with space group Fm-3m, consisting of a 3D framework of corner-shared octahedra with M^+ and M^{3+} alternatively in the center, Cl in the octahedra vertices thus forming MCl_6 and Cs in the external cavities among octahedra.

According to the extended Goldschmidt tolerance factor, Ag^+ and Na^+ have appropriate size for octahedral coordination of chloride or bromide ions in the perovskite lattice along with In^{3+}, Bi^{3+}, and Sb^{3+};[10,11] however, the Sb^{3+} compound shows a pronounced instability in air, thus making it a bad candidate for applications.[12]

B. Synthesis and Stability

Several strategies can be used to synthesize halide DPs in the form of powder and crystals. The most common synthetic approaches are based on hydrothermal methods,[13,14] supersaturation crystallization or solution precipitation, and solid-state reaction[13] (Fig. 2).

The hydrothermal method, with Teflon-lined stainless steel autoclave, allows the growth of mm-sized, high quality single crystals as reported by Luo *et al.* for $Cs_2AgInCl_6$ with trap density as low as 8.6×10^8 cm^{-3}.[15] In a typical synthesis procedure, metal chlorides are dissolved in a HCl solution and then heated in autoclave at

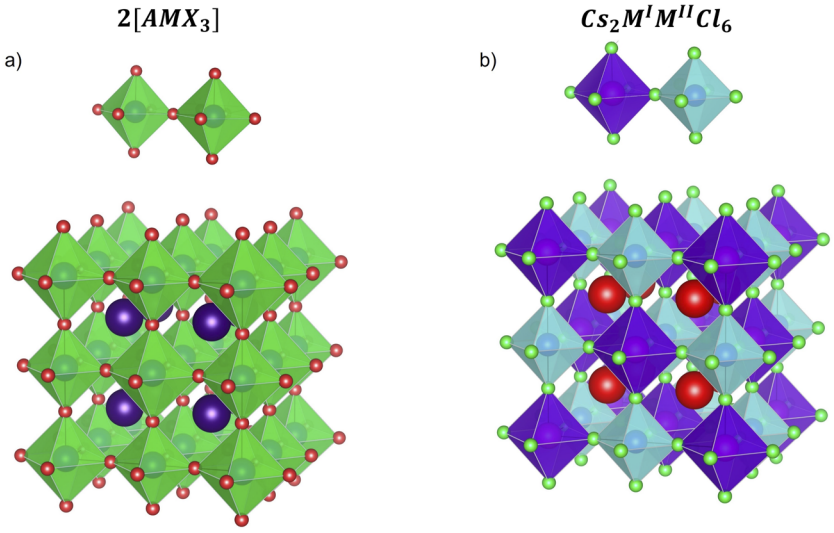

FIG. 1. (a) Perovskite AMX_3 crystal structure with X in red, A in violet, and M octahedrally coordinated. (b) Double perovskite (elpasolite) $Cs_2M^+M^{3+}Cl_6$ structure with space group Pm-3m with Cl in green and Cs in red and M^+/M^{3+} octahedrally coordinated.

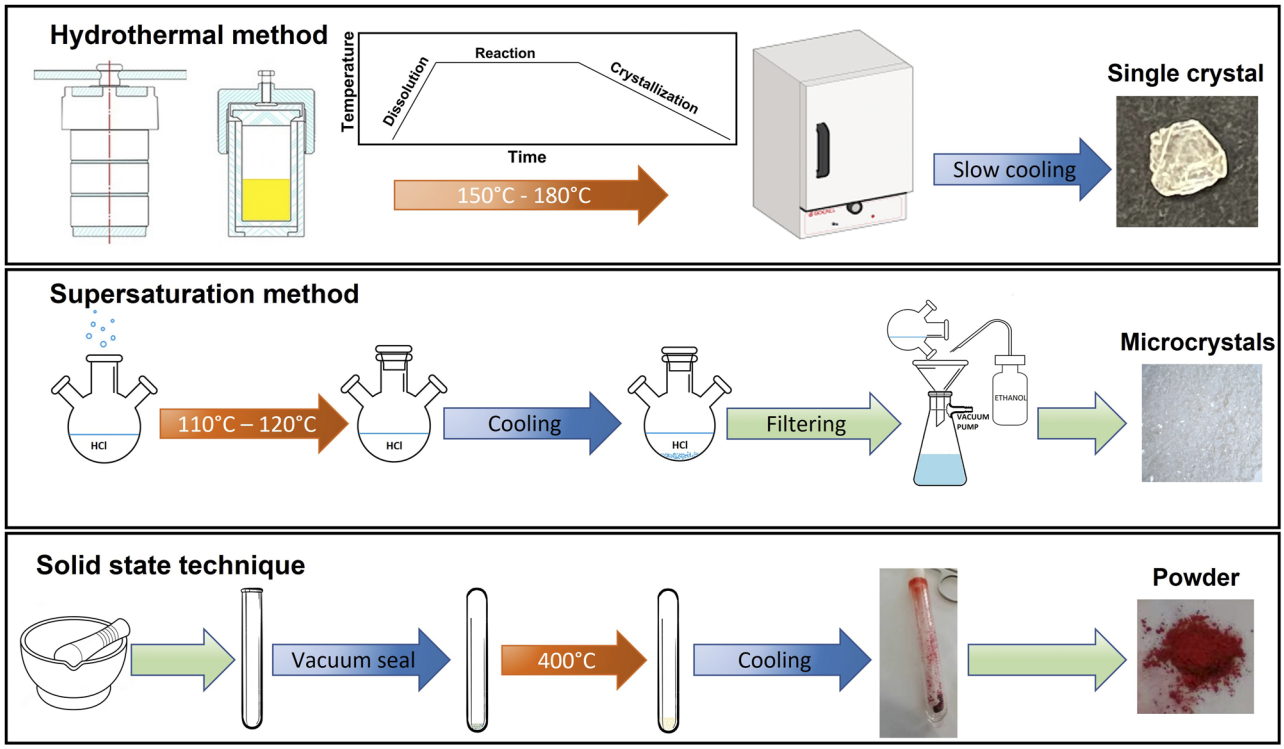

FIG. 2. Scheme of DPs synthesis techniques. Top: hydrothermal synthesis for large single crystals. Middle: supersaturation method for microcrystals. Bottom: solid state synthesis for powders.

150–180 °C with a subsequent slow cooling that determines the final size of the single crystal.

The supersaturation crystallization method is the simplest synthetic approach for the synthesis of microcrystals as it needs ambient conditions to dissolve precursor salts in the hydrohalic acid at relatively low temperature.[14] In a typical reaction, both metal chlorides and oxides can be used and dissolved in a HCl solution at 100 °C after vigorous stirring, and then the solution is cooled down. As the temperature decreases, the solution enters in a supersaturated state, and eventually crystals start to nucleate and grow. The size control of the products is therefore poor while the reproducibility of the pure phase is optimal.

Single-phase polycrystalline powders are mainly obtained by solid-state reaction in a fused silica ampoule.[16,17] The halide salts are mixed in appropriate molar ratio, and the ampoule is sealed under low pressure and heated typically around 500 °C for a few hours. More recently, a "green" synthesis under mild conditions has been developed.[18] In a typical reaction, two stable and transparent precursor solutions are prepared, one slightly acid with chlorides and the other one slightly basic with metal acetates. The formation of DPs occurs when the two solutions are mixed for a certain amount of time, without the use of high temperature or acids but with excess of proper cations during the reaction. All the possible substituting ions are proved to be incorporated uniformly into the DPs without phase separation.

Regardless of the synthetic method, inorganic halide DPs show excellent stability in ambient atmosphere over months, either in the dark or under illumination, even in the presence of moisture.[19,20] The thermal stability was also explored on microcrystals, and all the compositions are stable until 400 °C, while $Cs_2AgInCl_6$ is stable until 525 °C as no additional phase or decomposition signal in the XRD pattern was detected.[21,22]

Colloidal nanocrystals can be synthesized by the most common strategies, such as hot-injection method and antisolvent recrystallization, resulting in cubic nanocrystals with narrow size distribution. For more details, we refer to the several excellent reviews on DP colloidal nanocrystals and references therein.[23–25]

C. Optical properties of Na/Ag-In/Bi based DPs

The near unit emission efficiency of Na/Ag–In/Bi DPs is linked to the simultaneous presence of different ions in the same site. In their pure form, the two most stable undoped compounds $Cs_2AgInCl_6$ and $Cs_2NaInCl_6$ show a very low emission quantum yield. Volonakis *et al.*[26,27] synthesized $Cs_2AgInCl_6$ and, by combining first-principles calculations and experimental data, found out the direct nature of its bandgap and investigated the photoluminescence emission in the visible range under UV light. All the compounds with either Na^+ or Ag^+ in the monovalent site and In^{3+} in the trivalent site have direct and large bandgap (larger than 3 eV), and the

emission is broad-band in the visible range. Such compounds however show a nearly zero intrinsic photoluminescence quantum yield and the absorption at photon energies close to the bandgap edge is low.

The optical emission mechanism, with large Stokes shift and broadband emission, has been linked to the formation of self-trapped excitons (STEs), i.e., bound electron–hole pairs trapped by the distortion of the soft lattice induced by the presence of an electronic excited state.[28] After photoexcitation, an ultrafast transition occurs from a free exciton to an STE; the strong electron–phonon coupling favors the Jahn–Teller distortion of octahedra upon excitation, and consequently the optical emission from STEs occurs with a reduced photon energy with respect to the bandgap.[29]

The low emission quantum yield of the undoped $Cs_2AgInCl_6$ has been instead traced back to the parity-forbidden nature of inter-band transitions, related to a high symmetry lattice. The parity-forbidden transition between the valence band maximum (VBM) and the conduction band minimum (CBM) in $Cs_2AgInCl_6$ was analyzed by Meng *et al.* using density functional theory with Perdew–Burke–Ernzerhof (DFT-PBE) approach calculations[11] and by Liu *et al.*[30] by *ab initio* calculations with the Variational Pseudo-Self-Interaction corrected approach (VPSIC).[31] It was demonstrated that both the VBM and CBM lie at the Γ point, giving rise to a direct bandgap of about 2.1 eV and a parity-forbidden transition. The VBM is mainly constituted by Ag 4d and Cl 3p orbitals, while the CBM derives from unoccupied In 5s states. The calculated absorption coefficient is below 10^4 cm^{-1} and shows an onset with a tail about 1 eV long. Luo *et al.* experimentally observed two absorption edges: one at 2.1 eV that is parity-forbidden thus extremely weak, and the other one at 3.2 eV with a radiative recombination between electrons in CBM and holes in a lower level VBM-2, which is about 1.10 eV larger than the fundamental direct bandgap. The 3.2 eV transition is parity-allowed and shows a sharp absorption spectrum. These characteristics can explain the experimental optical bandgap of 3.2 eV with a photoluminescence emission energy of 2.1 eV[15] (see Table I).

Broadband emission with low efficiency is present in pure $Cs_2NaInCl_6$, but the partial substitution of Na with Ag bypasses the parity-forbidden transition and allows radiative recombination with higher efficiency, between 20% and 40% depending on the synthetic protocol. The emission properties studied by ultrafast spectroscopy demonstrated the presence of excitons trapped in long-lived dark states in the compound and very few bright STEs with nearly 100% radiative efficiency.[30]

The homologous compound $Cs_2NaBiCl_6$ shows slow conversion to $Cs_3Bi_2Cl_9$ when exposed to air;[12] therefore, the Bi^{3+} ion

TABLE I. Bandgap size and photoluminescence quantum yield in chloride DPs with various doping ions.

Compound	Dopant content	PLQY (%) PL max (nm)	Bandgap (eV) Direct	Bandgap (eV) Indirect	References
$Cs_2Na_{0.6}Ag_{0.4}InCl_6$	Bi^{3+} = 1%	97.7% (595)	3.08		30
	Bi^{3+} = 1%	97.3% (555)	6.42		32
	Bi^{3+} = 0,4%	86.2% (~550)	⋯		33
	Cu = 1%	62.6% (605)	2.3		34
	Bi^{3+} = 0.3%, Yb^{3+} = 13.6%	38.3% (1540)	⋯		35
	Sm = 35%	22% (540)		3.82	32
$Cs_2Na_{0.2}Ag_{0.8}InCl_6$	Mn 1%–100%	21%–41% (618)	3.67–3.82		32
	Yb^{3+} = 40%	46% (996) 82% (400-1100)	3.4		36
$Cs2AgIn_{0.7}Cr_{0.3}$ Cl_6	Yb^{3+} = 1%	45% (1000)	Direct		37
$Cs2Na_{1-x}Bi_{1-x}Mn_{2x}Cl_6$	x = 0.004	15% (590)	⋯		38
$Cs_2NaInCl_6$	Sb = 5%	79% (455)	5.1		39
	Bi^{3+}/Ho^{3+}	99% (455)	Direct		40
	0.1%–21.5%	72% (655)			41
	Yb^{3+} = 5.8%	39.4% (994)	⋯		
$Cs_2AgInCl_6$	⋯	⋯	3.23–3.53		27, 42, and 13
	Mn = 0.9%	3%–5% (619)			21
	Er^{3+} = 0.03–4%	7.9% (994 and 1540)			41
	Yb^{3+} = 6.9%				
$Cs_2AgBiCl_6$		⋯		2.2–2.77	1, 43, 14, and 44
$Cs_2AgSbCl_6$		⋯		2.24–2.61	13 and 42
$Cs_2AgSbBr_6$		⋯		1.64–1.93	45 and 46
$Cs_2AgBiBr_6$		⋯		1.70–2.25	47, 10, 19, 48, 14, 44, 49, 46, and 50

is considered more suitable as doping element than main component. In halide DPs, substitution of metal cations is one of the most efficient strategies to modify the emission properties and performance.

$Cs_2AgBiCl_6$ DP is also a stable compound, but it has indirect bandgap and has therefore very low emission yields. The whole range of possible intermediate compositions $Cs_2AgIn_{1-x}Bi_xCl_6$, with x varied from 0 to 1, has been explored, identifying precisely the transition from direct to indirect bandgap; the transition has been attributed to the band formed by the Bi 6s lone pair.[51,52]

In the following paragraphs, it will be discussed how the addition of such new elements helps breaking the parity rules and provides additional emission centers. In particular, starting from $Cs_2NaInCl_6$, it is possible to move to $Cs_2AgBiCl_6$ by gradually incorporating Ag^+ and Bi^{3+} during the synthesis, thus obtaining, for a well-defined composition, high efficient phosphors with PLQY approaching 100%.[53]

1. The role of Bi^{3+}

Luo *et al.* in 2018 studied the possibility to substitute chloride-based DPs with different metals in order to maximize the emission efficiency.[33] The most common composition for the highest emission efficiency is $Cs_2Na_{1-x}Ag_xIn_{1-y}Bi_yCl_6$ with variable x and y values. The simultaneous presence of In and Bi produces PLQY approaching 100%. The highest PLQY is obtained for 1% of Bi^{3+} substituted in the indium site, while a higher amount of the Bi ion causes self-quenching,[54] resulting in lower efficiency (see Fig. 3).

Several research groups have proposed an explanation for mechanism involved in the high PLQY, which is reported to be near 100% for $Cs_2Na_{0.6}Ag_{0.4}InCl_6$ +1% Bi^{3+}.

From the experimental point of view, in the presence of Bi, a new absorption peak appears at energies lower than the absorption in the pure matrix. The observation has been interpreted as evidence for the fact that the 6s states from Bi reside on top of the valence band and, given the abundance of s states from In at the bottom of the valence band, they significantly enhance the oscillator strength of optical transitions close to the band edge. In other words, the $6s^2$ lone pair is almost chemically inert, and thus it happens to be delocalized and resides within the energy gap of the matrix, ending up with a crucial role in optical transitions.[55]

From the structural point of view, solid-state nuclear magnetic resonance (NMR) spectroscopy reveals a high degree of ordering between M^+ and M^{3+} sites and a maximum PLQY is observed when bismuth is surrounded by 12 indium neighbors in its medium-range structure.[51]

Computational simulations by VPSIC show that the host material $Cs_2NaInCl_6$ has a large direct bandgap (see Table I) while $Cs_2AgInCl_6$ has a narrower bandgap, since the CBM is composed mainly by the indium 5s states and the VBM by the Ag 4d states. However, due to the already mentioned symmetry-forbidden transition between these states, the optical gap appears even larger. The addition of Bi produces a notable change in the band structure; indeed, the Bi 6s orbitals appear at the VBM and change its parity, increasing significantly optical absorption (Fig. 4).

Electronic structure calculations overwhelmingly deal with the ground state of the crystal, and thus they can be directly compared to experimental absorption spectra, since absorption starts from the ground state. Concerning optical emission, however, the process starts from the excited state, which is notoriously difficult to calculate, especially when, like in DPs, the electronic state couples strongly to the lattice degrees of freedom and produces polaronic distortions and self-trapping phenomena. For such a reason, it is extremely difficult to reproduce from first-principle calculations the broadband emission spectrum attributed to STEs. Concerning the role of Bi doping, the link between electronic structure calculations and photoluminescence emission quantum yield is therefore mostly qualitative. On one hand, the 6s Bi states at the top of the valence band are very likely to increase the oscillator strength for optical emission, much like they do for optical absorption.[30] On the other hand, other effects have been studied, like the role of Bi in passivating defects responsible for non-radiative decay of optical excitation,[29] or its ability to provide localized sites for efficient optical recombination.[56]

To further complicate matters, but also rendering them more interesting, the effect of Bi doping on the emission quantum yield is deeply intertwined in the presence of the other monovalent metal cations, namely, Ag and Na. Experimentally, some amount of each of these two elements is needed to achieve efficient emission. The role of Ag has been linked to the need to change the valence band parity and thus bypass the selection rules that forbid dipole transitions.[29,56] On the other hand, calculations show that Na orbitals do not contribute significantly to optical transitions close to the band-edge, so the role of Na appears to be more of a structural one, providing the spatial confinement of optical excitations that favors localization and self-trapping.[29]

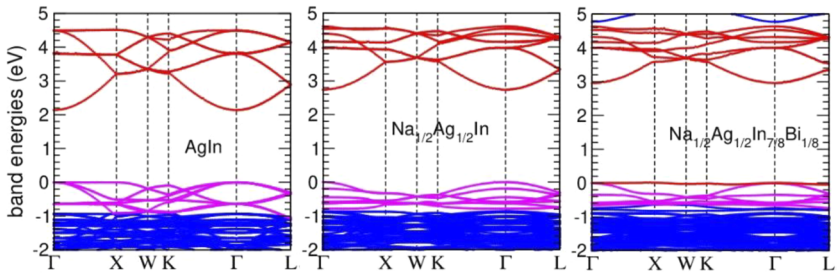

FIG. 3. VPSIC band energies calculated for various $Cs_2Na_{1-x}Ag_xIn_{1-y}Bi_yCl_6$ double perovskites; color code: red for conduction In s and valence Bi s bands; magenta for Ag 4d, e.g., bands, blue for Cl p and Bi p bands.

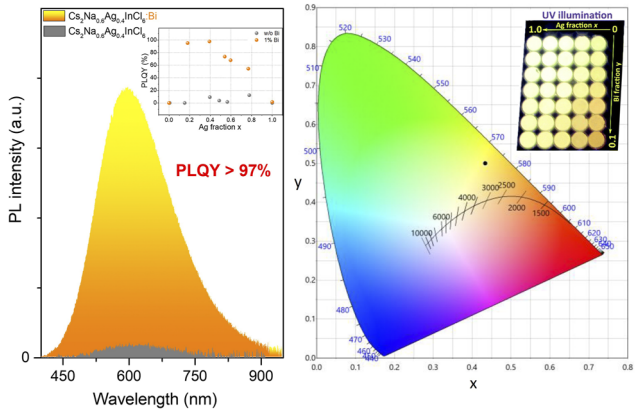

FIG. 4. Left panel: emission spectrum of $Cs_2Na_{0.6}Ag_{0.4}InCl_6$ (black) and $Cs_2Na_{0.6}Ag_{0.4}InCl_6$:Bi (orange). Inset: the PLQY for different Ag fraction. Right panel: CIE color map showing the position of the emission color of DP $Cs_2Na_{1-x}Ag_xIn_{1-y}Bi_yCl_6$ (y = 0.02, black point). Inset: photographs of a set of DP samples with varied x and y taken under UV illumination at 370–390 nm. Adapted with permission from Stroyuk et al., J. Mater. Chem. C **10**, 9938–9944 (2022). Copyright 2022 The Royal Society of Chemistry.

Ultrafast spectroscopy was used to explore the lifetime and recombination processes for the STEs in DPs. In particular, the comparison between transient absorption (TA) and time-resolved photoluminescence (TRPL) has highlighted the fact that long-lived STEs form independently of Bi doping, but the presence of Bi atoms transforms the STEs from almost completely dark to almost completely bright.[30] The minimum fraction of Bi^{3+} sufficient to turn STEs almost completely bright and thus achieve PLQY above 80% was measured to be less than 0.1%. The same ultrafast spectroscopy methods revealed that the presence of Ag is instead crucial to form STEs to begin with. Again, fractions as low as 1% of Ag atoms are sufficient to turn most of the optical excitations into STEs.

2. In^{3+} substitution with Sb^{3+}

Indirect bandgap is typically formed when lone-pair cations are present, e.g., in $Cs_2AgSbCl_6$,[57] while direct bandgap materials are obtained with In substituting Sb.[13] Nevertheless, some ions like Sb^{3+} are still attractive as dopant in direct bandgap compounds to improve the emission properties of DPs without affecting the absorption rate. The Sb^{3+} emission properties are strictly related to its crystallographic environment: in fivefold coordination, Sb^{3+} ions emit orange light while in six-fold coordination emit blue light.[58] The six-fold coordination radius of Sb^{3+} is suitable for incorporation in DPs as In^{3+} substitution without evident phase separation and, although it is slightly shorter than In^{3+}, the lattice parameter of chloride DP with increasing amount of Sb^{3+} is larger than the host In^{3+} matrix.[13,39]

The first report of blue emission involves the Sb^{3+} doping of $Cs_2NaInCl_6$.[59] The parity symmetries at the CBM and VBM in the bare $Cs_2NaInCl_6$ are the same, but the Sb^{3+} addition in the trivalent site produces a broadband blue emission at ≈450 nm with STE behavior and lifetime exceeding 1 μs.[60]

The incorporation of both Sb^{3+} and Bi^{3+} ions into $Cs_2NaInCl_6$, on the other hand, is able to generate a dual-emission blue and yellow light with a PLQY of 77%[61,62] originated by different $[SbCl_6]^{3-}$ distortions related to STEs (Fig. 5). Surprisingly, the Sb^{3+} doped DP shows improved thermal stability with respect to the undoped counterpart, with a decomposition temperature of 600 °C and an excellent stability under environmental conditions and illumination.[59]

3. In^{3+} substitution with lanthanides

The octahedral site of DPs is also suitable for incorporation of lanthanide (Ln^{3+}) ions, such as Yb^{3+} and Er^{3+}, Nd^{3+}, Ho^{3+}, and Tm^{3+}. The presence of such ions endows DPs with sharp atomic-like optical transitions, often covering the near-infrared (NIR) wavelength bands that are relevant for solid-state lasers (e.g., the 1 μm emission from Yb^{3+} and Nd^{3+}) and optical communications (1.55 μm emission from Er^{3+}).

Yb^{3+} ions have a simple f-electronic structure, involving only two multiplets responsible for a single ($^2F_{5/2} \rightarrow {}^2F_{7/2}$) transition manifold in the NIR range, at ~1 μm wavelength. Mahor *et al.* synthesized Yb^{3+}-doped $Cs_2AgInCl_6$ microcrystals and studied the emission properties.[63] The incorporation of Yb^{3+} ions in the DP matrix was below 2% and the NIR photoluminescence showed millisecond-long lifetimes that are close to the intrinsic radiative limit upon UV light excitation, via energy transfer from the

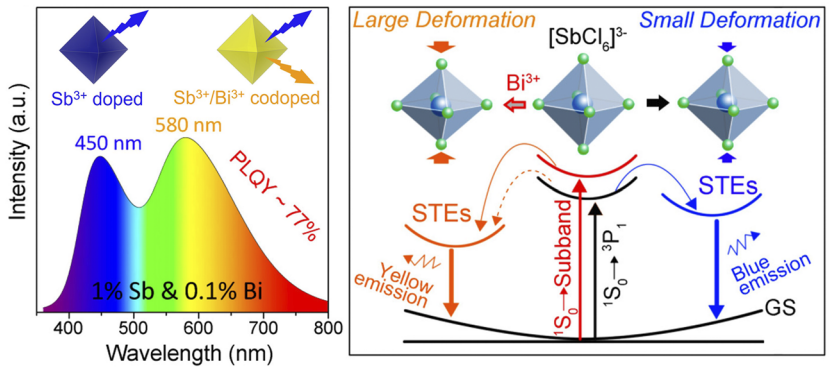

FIG. 5. Dual-emission white-light PL in Sb^{3+}/Bi^{3+} co-doped single crystals and schematic of the energy level structure of blue and yellow emissive self-trapped excitons. Adapted with permission from Zhou *et al.*, ACS Energy Lett. **6**, 3343–3351 (2021). Copyright 2021 American Chemical Society.

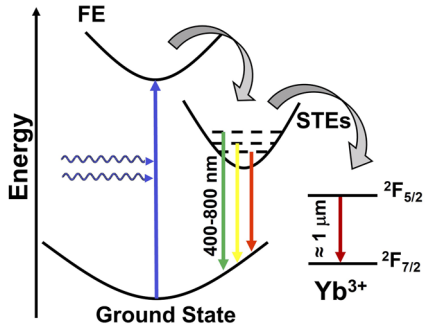

FIG. 6. Energy diagram of lanthanide-based DPs, highlighting energy transfer from self-trapped exciton states to Yb^{3+} electronic states followed by Yb^{3+} emission around 1 μm. Yb^{3+} electronic states are labeled using spectroscopic notation.

host matrix absorbing the light to the f-electron states of the lanthanide. The efficient Yb^{3+} emission was traced back to the low energy distribution of the DP phonon modes, resulting in negligible non-radiative losses.[64]

Bi^{3+} and Ln^{3+} co-doping is effective in enhancing the optical emission performance of DPs, both in terms of spectral range and quantum efficiency. Based on the $Cs_2Na_{0.6}Ag_{0.4}InCl_6$ host matrix, Bi^{3+} and Yb^{3+} co-doping was shown to result in a dual emission consisting of highly efficient, warm-white emission from the STEs and 1 μm emission from the Yb^{3+} ions.[65] The underlying mechanism is an energy transfer process from the STEs of the DP matrix to the Yb^{3+} ions, as represented in the scheme of Fig. 6. Similarly, Er^{3+}-doping allows for multiple characteristic emission lines spanning the visible and the NIR, arising from the optical transitions $^2H_{11/2} \rightarrow {}^4I_{15/2}$ (525 nm), $^4S_{3/2} \rightarrow {}^4I_{15/2}$ (550 nm), $^4F_{9/2} \rightarrow {}^4I_{15/2}$ (665 nm), $^4I_{9/2} \rightarrow {}^4I_{15/2}$ (805 nm), and $^4I_{13/2} \rightarrow {}^4I_{15/2}$ (1540 nm).[35,41,66] As a matter of fact, the presence of Bi^{3+} is crucial to realizing strong emission from lanthanides through STE-to-Ln^{3+} energy transfer.[66] Quite importantly, concentration quenching effects was found to occur in Er^{3+}-doped DPs as the ion concentration reaches up to values larger than 18%.[35]

Yb^{3+}-doped DPs also represent a promising platform for highly sensitive thermal detection as the dual-emission from STEs and Yb^{3+} ions can be modified by tuning the energy transfer between the two emission centers. In fact, the intensity of the Yb^{3+} NIR PL is sensitive to the lattice temperature and decreases with increasing temperature, whereas its lifetime exhibits only a negligible temperature sensitivity.[67] In addition, the visible emission from STEs is highly sensitive to the temperature, and its lifetime decreases sensibly with increasing temperature, which reflects on the energy transfer to Yb^{3+} levels. The STE/Yb^{3+} PL intensity ratio turns out to be an effective parameter for optical thermometer sensitivity. Simultaneous doping with Er^{3+} ions, whose emission is sensitized via cascaded energy transfer, can be exploited to further increase the materials thermal sensitivity.[68]

By doping the host matrix with multiple NIR Ln^{3+}, such as Nd, Yb, Er, and Tm, Chen's group realized a material with ultrabroad band emission from the visible to the NIR, covering the 400–2000 nm emission range.[69] Again, the multiband emission from the lanthanides arises from cascaded energy transfer starting from STEs through the lanthanide electronic levels. A compact light source was also fabricated with the Ln-doped DP coupled with a commercial UV LED chip to obtain an ultrabroad emission as shown in Fig. 7.

4. Transition-metal ions: Mn^{2+}, Cr^{3+}, Fe^{3+}

In the case of Mn-doping, the ion involved is divalent (Mn^{2+}) and can replace both Ag^+ and In^{3+} in the $Cs_2AgInCl_6$ lattice, generating a new optical emission in the visible range. The host materials is able to transfer the excitation energy from the UV absorbed light to the Mn d-electrons and the de-excitation of Mn d-electrons generates a PL emission centered at ≈ 600 nm with the highest PLQY reaching 5% for the 0.9% doped DP.[21,70]

On the other hand, the host DP for Mn^{2+} doping can be $Cs_2NaBiCl_6$ as studied by Majher *et al.*[38] giving an orange-red emis-

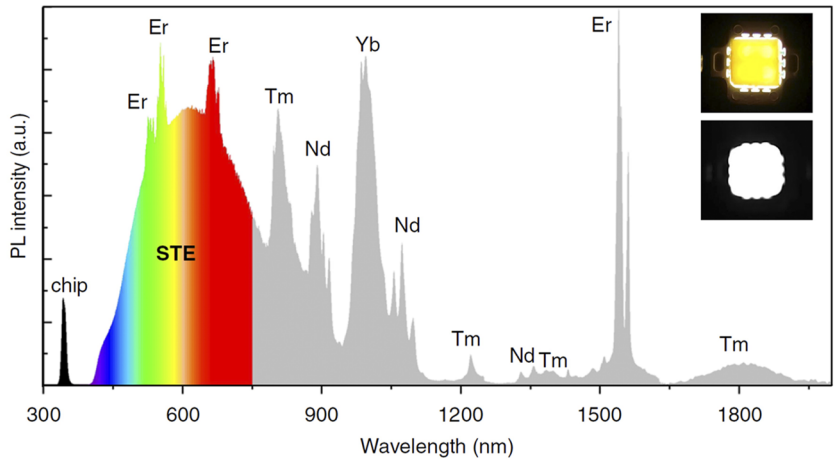

FIG. 7. Ultrabroadband LED based on Bi^{3+}/Ln^{3+} co-doped DP. PL spectrum of the corresponding LED device with an operating current of 200 mA. Inset: Photographs of the LED taken by visible-light camera and NIR camera. Adapted with permission from Jin *et al.*, Light: Sci. Appl. **11**, 52 (2022). Copyright 2022, Author(s).

sion with ≈15% quantum yield. The proposed emission mechanism considers Bi^{3+} ion as the absorption site for UV light whose energy is transferred to Mn^{2+} that emits light centered at 590 nm.

A more recent study reports Mn^{2+}-doped $Cs_2AgBiCl_6$ with an accurate structural study along with the stability of this material confirming the emission in the orange-red range (601 nm) due to the d-d transitions of Mn.[71]

Trivalent chromium ions can be incorporated in $Cs_2AgInCl_6$ matrix as substitution of In^{3+} sites in octahedral coordination to obtain a broadband emission in the NIR range. The 3d energy levels of Cr^{3+} have found to be responsible for the emission in the 850–1350 nm range through the spin-allowed $^4T_2 \rightarrow {}^4A_2$ transition and the overall PLQY is ≈ 22%.[16] The co-doping with Cr^{3+} and Yb^{3+} is effective to improve the PLQY up to 45% in the same NIR range.[37] The enhanced efficiency is attributed to a better crystallinity of the matrix that leads to a more effective energy transfer from STEs states to Cr^{3+} levels analogously to the already described process in Yb^{3+}-doped compounds and reduced non-radiative recombination.

A different behavior is found in Fe^{3+} doping of $Cs_2AgInCl_6$, which is able to reduce the bandgap down to 1.6 eV, making it more suitable for photovoltaic applications. Nevertheless, at the atomic level, Fe^{3+} is found to replace In^{3+} and segregate the matrix in iron-rich homogeneously distributed microscopic domains of different size, depending of the Fe^{3+} substitution level.[72] The total substitution of In^{3+} with Fe^{3+} leads to a bandgap of 1.55 eV and an efficient exciton dissociation that is promising for photovoltaic applications.[73]

III. BROMIDE DOUBLE PEROVSKITE: $Cs_2AgBiBr_6$

Besides chloride-based DPs, bromide-based ones have been studied recently as candidates for lead-free and stable solar cells, thanks to their lower bandgap and the possibility to obtain thin films by spin coating. However, most bromide DPs happen to be unstable. The only compound that was found to be relatively stable is $Cs_2AgBiBr_6$, but it has indirect bandgap that limits light absorption. In addition, carrier mobility is low and lifetime is short, possibly due to the strong electron–phonon coupling, and consequently prototype solar cells have shown low photoconversion efficiency. Several attempts have been made to improve the optoelectronic properties of bromide DPs, such as optimization of film deposition to diminish the concentration of defects states or doping with other elements to reduce the bandgap, but the solar cell efficiency is still below 5%.[10,74–77]

By controlling the temperature during the growth of $Cs_2AgBiBr_6$ single crystals, Gao *et al.* were able to reduce the bandgap of 0.26 eV possibly caused by an increased level of Ag/Bi disorder.[78] The partial replacement of Ag^+ ions by Cu^+ ions is reported to show enhanced NIR absorption in single crystals.[79] However, a single crystal is not suitable to be integrated in a device such a solar cell. Very recently, Zhang *et al.* developed a specific doping with atomic hydrogen that reduced the film bandgap down to 1.64 eV.[80] The hydrogenation process resulted in doping atoms occupying interstitial sites and thus modifying the VB and CB levels through coupling with the perovskite cations. The highest solar cell photoconversion efficiency after hydrogenation was 6.37%, stable under illumination.

In Br-based DPs the incorporation of new ions could be employed to introduce additional physical properties. Magnetic Fe^{3+}, added during the synthesis through $FeBr_3$, replaces Bi^{3+} and forms $FeBr_6$ homogeneously distributed clusters in the lattice and, besides extending the absorption to 800 nm thanks to bandgap narrowing, shows ferromagnetic or antiferromagnetic response that could be promising for spintronic devices.[81] Furthermore, introducing Fe^{3+} through $FeBr_2$ during the synthesis is reported to generate a new intermediate band that broadens the absorption to 1350 nm. Additionally, photocurrent is generated under NIR irradiation that makes this materials promising both in NIR photodetector and solar cells.[82]

When doped with Yb^{3+}, $Cs_2AgBiBr_6$ shows outstanding emission properties with PLQY up to 95% and a good stability in air. The mechanism for the emission through Yb^{3+} is analogous to energy transfer in chloride-based DPs. After optical excitation, electrons transfer to a nearby Yb^{3+} ion, which emit efficiently in the NIR region through the $^2F_{5/2} \rightarrow {}^2F_{7/2}$ electronic transition.[83,84]

IV. CONCLUSION, CHALLENGES, AND PERSPECTIVES

The most promising field of application for chloride DPs is lighting, since they happen to be the best possible phosphor or emitter materials emitting warm white light with a spectrum almost perfectly fit for human vision and high color rendering, all with quantum efficiencies approaching unity. Furthermore, DPs are stable in air and they retain their emission spectrum and quantum yield for as long as they are tested, even if they are submersed in water. The materials platform of DPs is very flexible and can accommodate many different elements, but the optical properties are very robust against variations in stoichiometry; the warm white light emission spectrum and the high quantum yield depend on the presence of various elements in the composition, but not on their exact amounts. DPs can be engineered to emit efficiently also in the blue spectral region and in the near IR, opening to interesting prospects as laser materials, as well as optical markers in microscopy and biology.

Most optoelectronic applications, such as the realization of LEDs and lasers, require the fabrication of thin films, which is one of the main challenges of the moment. Powders and microcrystals are stable and easy to obtain, but their potential use in light emissive devices is limited due to the presence of intense light scattering. Producing high-quality thin films appear to be much more challenging, since chloride-based DPs are poorly soluble in solvents and not solution-processable. A possible option is represented by low pressure thermal-evaporation, which has been successfully demonstrated, although resulting in PLQY limited to 10%–15%. Very recently, Stroyuk *et al.* were able to deposit stable and transparent films from microcrystalline $Cs_2Ag_xNa_{1-x}Bi_yIn_{1-y}Cl_6$ with partially preserved PLQY reaching 85%.[85] Colloidal nanocrystals can be used as inks for the deposition of films; however, PLQY in such a form is currently lower than in the bulk counterpart probably due to un-passivated surface states or reduced electron–phonon coupling.

It should be remarked that such limitations may be moot or at least not too severe for the application as phosphors, since DPs are transparent in the visible region, and therefore microcrystals can be successfully incorporated in an inorganic glass matrix with similar refractive index to form a composite to be layered on a commercial UV LED chip to convert blue and UV light into warm white one.

Doping with lanthanides, on the other hand, allows us to obtain an ultrabroad emission band from the visible range to the NIR range for applications in spectroscopic analysis and multifunctional lighting or non-destructive biomedical imaging. The emission from Yb, due to the energy transfer from STEs, has both intensity and lifetime steeply dependent on temperature and can be applied for the development of highly sensitive optical thermometers.[67]

Further investigations are needed to optimize the integration in emissive devices both in the case of pure DP films and composites. The research perspective emphasizes the need for advancing film processing techniques specific to chloride DPs with all the possible ion substitutions. This involves developing methods for directly converting highly efficient powders or microcrystals into optically transparent films and improving the composite materials to preserve high quantum yield.

Any time halide perovskite structure is mentioned, materials are automatically considered promising for photovoltaics. In the case of DP, however, the prospects for photoconversion of sunlight into electric current do not appear particularly good: the bandgap of most compound is way too high for reasonable efficiency so that a very small fraction of solar photons may be absorbed. Furthermore, optical emission at photon energies well below the bandgap demonstrates that excited states may dissipate most of the photon energy before carrier extraction. To be useful as photovoltaic materials, new DPs will have to be synthesized, with much lower bandgap and possibly with a weaker coupling between electronic excitations and lattice deformation, in order to inhibit self-trapping phenomena.

ACKNOWLEDGMENTS

This work was funded by Fondazione di Sardegna through Project No. 2F20000210007 "Perovskite materials for photovoltaics" and Project No. F73C22001160007 "Single crystal hybrid perovskite thin films for optoelectronics." A.S. was supported by PON "Ricerca e Innovazione" 2014–2020—Fondo sociale europeo, Attraction and International Mobility—Codice AIM1809115 Num. Attività 2, Linea 2.1. Funding is acknowledged under the National Recovery and Resilience Plan (NRRP), Mission 4 Component 2 Investment 1.3 - Call for tender No. 1561 of October 11, 2022 of Ministero dell'Università e della Ricerca (MUR); funded by the European Union – NextGenerationEU, Project code PE0000021, Concession Decree No. 1561 of October 11, 2022 adopted by Ministero dell'Università e della Ricerca (MUR), CUP – F53C220007700077, according to attachment E of Decree No. 1561/2022, Project title "Network 4 Energy Sustainable Transition—NEST."

AUTHOR DECLARATIONS

Conflict of Interest

The authors have no conflicts to disclose.

Author Contributions

Daniela Marongiu: Supervision (equal); Writing – original draft (equal); Writing – review & editing (equal). **Stefano Lai**: Writing – original draft (equal). **Fang Liu**: Writing – review & editing (equal). **Angelica Simbula**: Writing – review & editing (supporting). **Francesco Quochi**: Writing – original draft (equal); Writing – review & editing (equal). **Michele Saba**: Writing – original draft (equal); Writing – review & editing (equal). **Andrea Mura**: Writing – review & editing (supporting). **Giovanni Bongiovanni**: Writing – original draft (equal); Writing – review & editing (equal).

DATA AVAILABILITY

Data sharing is not applicable to this article as no new data were created or analyzed in this study.

REFERENCES

[1] J. Cho, J. H. Park, J. K. Kim, and E. F. Schubert, "White light-emitting diodes: History, progress, and future," Laser Photonics Rev. **11**, 1600147 (2017).
[2] Y. Liu, A. Nag, L. Manna, and Z. Xia, "Lead-free double perovskite $Cs_2AgInCl_6$," Angew. Chem., Int. Ed. **60**, 11592–11603 (2021).
[3] O. Stroyuk, O. Raievska, J. Hauch, and C. J. Brabec, "Doping/alloying pathways to lead-free halide perovskites with ultimate photoluminescence quantum yields," Angew. Chem., Int. Ed. **62**, 202212668 (2022).
[4] Z. Xiao, Z. Song, and Y. Yan, "From lead halide perovskites to lead-free metal halide perovskites and perovskite derivatives," Adv. Mater. **31**, 1803792 (2019).
[5] N. R. Wolf, B. A. Connor, A. H. Slavney, and H. I. Karunadasa, "Doubling the stakes: The promise of halide double perovskites," Angew. Chem., Int. Ed. **60**, 16264–16278 (2021).
[6] V. M. Goldschmidt, "Die gesetze der krystallochemie," Naturwissenschaften **14**, 477–485 (1926).
[7] W. Travis, E. N. K. Glover, H. Bronstein, D. O. Scanlon, and R. G. Palgrave, "On the application of the tolerance factor to inorganic and hybrid halide perovskites: A revised system," Chem. Sci. **7**, 4548–4556 (2016).
[8] C. J. Bartel *et al.*, "New tolerance factor to predict the stability of perovskite oxides and halides," Sci. Adv. **5**, eaav0693 (2019).
[9] I. N. Flerov *et al.*, "Phase transitions in elpasolites (ordered perovskites)," Mater. Sci. Eng., R **24**, 81–151 (1998).
[10] A. H. Slavney, T. Hu, A. M. Lindenberg, and H. I. Karunadasa, "A bismuth-halide double perovskite with long carrier recombination lifetime for photovoltaic applications," J. Am. Chem. Soc. **138**, 2138–2141 (2016).
[11] W. Meng *et al.*, "Parity-forbidden transitions and their impact on the optical absorption properties of lead-free metal halide perovskites and double perovskites," J. Phys. Chem. Lett. **8**, 2999–3007 (2017).
[12] W. M. A. Smit, G. J. Dirksen, and D. J. Stufkens, "Infrared and Raman spectra of the elpasolites $Cs_2NaSbCl_6$ and $Cs_2NaBiCl_6$: Evidence for a pseudo Jahn-Teller distorted," J. Phys. Chem. Solids **51**, 189–196 (1990).
[13] T. T. Tran, J. R. Panella, J. R. Chamorro, J. R. Morey, and T. M. McQueen, "Designing indirect-direct bandgap transitions in double perovskites," Mater. Horiz. **4**, 688–693 (2017).
[14] M. R. Filip, S. Hillman, A. A. Haghighirad, H. J. Snaith, and F. Giustino, "Band gaps of the lead-free halide double perovskites $Cs_2BiAgCl_6$ and $Cs_2BiAgBr_6$ from theory and experiment," J. Phys. Chem. Lett. **7**, 2579–2585 (2016).
[15] J. Luo *et al.*, "$Cs_2AgInCl_6$ double perovskite single crystals: Parity forbidden transitions and their application for sensitive and fast UV photodetectors," ACS Photonics **5**, 398–405 (2018).
[16] F. Zhao, Z. Song, J. Zhao, and Q. Liu, "Double perovskite $Cs_2AgInCl_6$:Cr^{3+}: Broadband and near-infrared luminescent materials," Inorg. Chem. Front. **6**, 3621–3628 (2019).
[17] Z. Xiao *et al.*, "Intrinsic instability of $Cs_2In(I)M(III)X_6$ (M = Bi, Sb; X = halogen) double perovskites: A combined density functional theory and experimental study," J. Am. Chem. Soc. **139**, 6054–6057 (2017).
[18] O. Stroyuk *et al.*, "'Green' synthesis of highly luminescent lead-free $Cs_2Ag_xNa_{1-x}Bi_yIn_{1-y}Cl_6$ perovskites," J. Mater. Chem. C **10**, 9938–9944 (2022).

[19]E. T. McClure, M. R. Ball, W. Windl, and P. M. Woodward, "Cs_2AgBiX_6 (X = Br, Cl): New visible light absorbing, lead-free halide perovskite semiconductors," Chem. Mater. **28**, 1348–1354 (2016).
[20]J. Zhou, X. Rong, M. S. Molokeev, X. Zhang, and Z. Xia, "Exploring the transposition effects on the electronic and optical properties of $Cs_2AgSbCl_6$: Via a combined computational-experimental approach," J. Mater. Chem. A **6**, 2346–2352 (2018).
[21]K. Nila Nandha and A. Nag, "Synthesis and luminescence of Mn-doped $Cs_2AgInCl_6$ double perovskites," Chem. Commun. **54**, 5205–5208 (2018).
[22]Z. Xiao, W. Meng, J. Wang, and Y. Yan, "Thermodynamic stability and defect chemistry of bismuth-based lead-free double perovskites," ChemSusChem **9**, 2628–2633 (2016).
[23]B. Yang *et al.*, "Lead-free direct band gap double-perovskite nanocrystals with bright dual-color emission," J. Am. Chem. Soc. **140**, 17001–17006 (2018).
[24]F. Locardi *et al.*, "Colloidal synthesis of double perovskite $Cs_2AgInCl_6$ and Mn-doped $Cs_2AgInCl_6$ nanocrystals," J. Am. Chem. Soc. **140**, 12989–12995 (2018).
[25]Y. Liu, Y. Jing, J. Zhao, Q. Liu, and Z. Xia, "Design optimization of lead-free perovskite $Cs_2AgInCl_6$:Bi nanocrystals with 11.4% photoluminescence quantum yield," Chem. Mater. **31**, 3333–3339 (2019).
[26]G. Volonakis, A. A. Haghighirad, H. J. Snaith, and F. Giustino, "Route to stable lead-free double perovskites with the electronic structure of $CH_3NH_3PbI_3$: A case for mixed-cation $[Cs/CH_3NH_3/CH(NH_2)_2]_2InBiBr_6$," J. Phys. Chem. Lett. **8**, 3917–3924 (2017).
[27]G. Volonakis *et al.*, "$Cs_2InAgCl_6$: A new lead-free halide double perovskite with direct band gap," J. Phys. Chem. Lett. **8**, 772–778 (2017).
[28]X. Wang *et al.*, "Atomistic mechanism of broadband emission in metal halide perovskites," J. Phys. Chem. Lett. **10**, 501–506 (2019).
[29]S. Li, J. Luo, J. Liu, and J. Tang, "Self-trapped excitons in all-inorganic halide perovskites: Fundamentals, status, and potential applications," J. Phys. Chem. Lett. **10**, 1999–2007 (2019).
[30]F. Liu *et al.*, "White light emission with unity efficiency from $Cs_2Na_{1-x}Ag_xIn_{1-y}Bi_yCl_6$ double perovskites: The role of bismuth and silver," J. Mater. Chem. C **10**, 14232–14241 (2022).
[31]A. Filippetti *et al.*, "Variational pseudo-self-interaction-corrected density functional approach to the *ab initio* description of correlated solids and molecules," Phys. Rev. B: Condens. Matter Mater. Phys. **84**, 195127 (2011).
[32]K. Peng *et al.*, "The synthesis of lead-free double perovskite $Cs_2Ag_{0.4}Na_{0.6}InCl_6$ phosphor with improved optical properties via ion doping," J. Alloys Compd. **891**, 161978 (2022).
[33]J. Luo *et al.*, "Efficient and stable emission of warm-white light from lead-free halide double perovskites," Nature **563**, 541–545 (2018).
[34]X. Cheng *et al.*, "Boosting the self-trapped exciton emission in alloyed $Cs_2(Ag/Na)InCl_6$ double perovskite via Cu^+ doping," Adv. Sci. **9**, 2103724 (2022).
[35]J. Zhao *et al.*, "Efficient dual-mode emissions of high-concentration erbium ions doped lead-free halide double perovskite single crystals," J. Alloys Compd. **895**, 162601 (2022).
[36]N. Liu *et al.*, "Near-infrared afterglow and related photochromism from solution-grown perovskite crystal," Adv. Funct. Mater. **32**, 2110663 (2022).
[37]D. Chen *et al.*, "Simultaneous enhancement of near infrared luminescence and stability of $Cs_2AgInCl_6$:Cr^{3+} double perovskite single crystals enabled by a Yb^{3+} dopant," Inorg. Chem. Front. **9**, 4695–4704 (2022).
[38]J. D. Majher, M. B. Gray, T. A. Strom, and P. M. Woodward, "$Cs_2NaBiCl_6$:Mn^{2+}—A new orange-red halide double perovskite phosphor," Chem. Mater. **31**, 1738–1744 (2019).
[39]M. B. Gray *et al.*, "High-efficiency blue photoluminescence in the $Cs_2NaInCl_6$:Sb^{3+} double perovskite phosphor," J. Mater. Chem. C **8**, 6797–6803 (2020).
[40]J. Nie *et al.*, "Efficient red photoluminescence in holmium-doped $Cs_2NaInCl_6$ double perovskite," Cell Rep. Phys. Sci. **3**, 100820 (2022).
[41]S. Han *et al.*, "Unveiling local electronic structure of lanthanide-doped $Cs_2NaInCl_6$ double perovskites for realizing efficient near-infrared luminescence," Adv. Sci. **9**, 2203735 (2022).
[42]J. Zhou *et al.*, "Composition design, optical gap and stability investigations of lead-free halide double perovskite $Cs_2AgInCl_6$," J. Mater. Chem. A **5**, 15031–15037 (2017).
[43]G. Volonakis *et al.*, "Lead-free halide double perovskites via heterovalent substitution of noble metals," J. Phys. Chem. Lett. **7**, 1254–1259 (2016).
[44]R. L. Z. Hoye *et al.*, "Fundamental carrier lifetime exceeding 1 μs in $Cs_2AgBiBr_6$ double perovskite," Adv. Mater. Interfaces **5**, 1800464 (2018).
[45]F. Wei *et al.*, "Enhanced visible light absorption for lead-free double perovskite $Cs_2AgSbBr_6$," Chem. Commun. **55**, 3721–3724 (2019).
[46]Y. El Ajjouri *et al.*, "Mechanochemical synthesis of Sn(II) and Sn(IV) iodide perovskites and study of their structural, chemical, thermal, optical, and electrical properties," Energy Technol. **8**, 1900788 (2020).
[47]A. D. Wright *et al.*, "Ultrafast excited-state localization in $Cs_2AgBiBr_6$ double perovskite," J. Phys. Chem. Lett. **12**, 3352–3360 (2021).
[48]Q. Li *et al.*, "High-pressure band-gap engineering in lead-free $Cs_2AgBiBr_6$ double perovskite," Angew. Chem., Int. Ed. **56**, 15969–15973 (2017).
[49]S. J. Zelewski *et al.*, "Revealing the nature of photoluminescence emission in the metal-halide double perovskite $Cs_2AgBiBr_6$," J. Mater. Chem. C **7**, 8350–8356 (2019).
[50]F. Ji *et al.*, "Lead-free halide double perovskite $Cs_2AgBiBr_6$ with decreased band gap," Angew. Chem., Int. Ed. **59**, 15191–15194 (2020).
[51]A. Karmakar, G. M. Bernard, A. Meldrum, A. O. Oliynyk, and V. K. Michaelis, "Tailorable indirect to direct band-gap double perovskites with bright white-light emission: Decoding chemical structure using solid-state NMR," J. Am. Chem. Soc. **142**, 10780–10793 (2020).
[52]K. Z. Du, W. Meng, X. Wang, Y. Yan, and D. B. Mitzi, "Bandgap engineering of lead-free double perovskite $Cs_2AgBiBr_6$ through trivalent metal alloying," Angew. Chem., Int. Ed. **56**, 8158–8162 (2017).
[53]O. Stroyuk *et al.*, "$Cs_2Ag_xNa_{1-x}Bi_yIn_{1-y}Cl_6$ perovskites approaching photoluminescence quantum yields of 100%," Mater. Adv. **3**, 7894–7903 (2022).
[54]J. Li *et al.*, "Antimony doped Cs_2SnCl_6 with bright and stable emission," Front. Optoelectron. **12**, 352–364 (2019).
[55]K. M. McCall, V. Morad, B. M. Benin, and M. V. Kovalenko, "Efficient lone-pair-driven luminescence: Structure-property relationships in emissive $5s^2$ metal halides," ACS Mater. Lett. **2**, 1218–1232 (2020).
[56]F. Locardi *et al.*, "Emissive Bi-doped double perovskite $Cs_2Ag_{1-x}Na_xInCl_6$ nanocrystals," ACS Energy Lett. **4**, 1976–1982 (2019).
[57]A. Karmakar, M. S. Dodd, S. Agnihotri, E. Ravera, and V. K. Michaelis, "Cu(II)-doped $Cs_2SbAgCl_6$ double perovskite: A lead-free, low-bandgap material," Chem. Mater. **30**, 8280–8290 (2018).
[58]Y. Jing *et al.*, "Sb^{3+} dopant and halogen substitution triggered highly efficient and tunable emission in lead-free metal halide single crystals," Chem. Mater. **32**, 5327–5334 (2020).
[59]R. Zeng *et al.*, "Highly efficient blue emission from self-trapped excitons in stable Sb^{3+}-doped $Cs_2NaInCl_6$ double perovskites," J. Phys. Chem. Lett. **11**, 2053–2061 (2020).
[60]A. Noculak *et al.*, "Bright blue and green luminescence of Sb(III) in double perovskite Cs_2MInCl_6(M = Na, K) matrices," Chem. Mater. **32**, 5118–5124 (2020).
[61]B. Zhou *et al.*, "Efficient white photoluminescence from self-trapped excitons in Sb^{3+}/Bi^{3+}-codoped $Cs_2NaInCl_6$ double perovskites with tunable dual-emission," ACS Energy Lett. **6**, 3343–3351 (2021).
[62]M. Liu, C.-K. Duan, P. A. Tanner, C.-G. Ma, and M. Yin, "Rationalizing the photoluminescence of Bi^{3+} and Sb^{3+} in double perovskite halide crystals," J. Phys. Chem. C **125**, 26670–26678 (2021).
[63]Y. Mahor, W. J. Mir, and A. Nag, "Synthesis and near-infrared emission of Yb-doped $Cs_2AgInCl_6$ double perovskite microcrystals and nanocrystals," J. Phys. Chem. C **123**, 15787 (2019).
[64]P. A. Loiko *et al.*, "Stokes and anti-Stokes luminescence from cubic elpasolite Cs_2NaYF_6 crystals doped with Er^{3+} and Yb^{3+} ions," J. Lumin. **175**, 260–266 (2016).
[65]G. Zhang *et al.*, "Facile solution synthesis of Bi^{3+}/Yb^{3+} ions co-doped $Cs_2Na_{0.6}Ag_{0.4}InCl_6$ double perovskites with near-infrared emission," Dalton Trans. **49**, 15231–15237 (2020).
[66]H. Arfin, J. Kaur, T. Sheikh, S. Chakraborty, and A. Nag, "Bi^{3+}–Er^{3+} and Bi^{3+}–Yb^{3+} codoped $Cs_2AgInCl_6$ double perovskite near-infrared emitters," Angew. Chem., Int. Ed. **59**, 11307–11311 (2020).

[67] S. Yang *et al.*, "Bi and Yb codoped $Cs_2Ag_{0.6}Na_{0.4}InCl_6$ microcrystals: Visible to near-infrared fluorescence for thermometry," J. Phys. Chem. C **125**, 10431–10440 (2021).
[68] Z. Xu *et al.*, "Yb/Er: $Cs_2Ag(In/Bi)Cl_6$ lead-free double perovskite for dual-modal optical temperature sensing," J. Lumin. **248**, 118996 (2022).
[69] S. Jin *et al.*, "Compact ultrabroadband light-emitting diodes based on lanthanide-doped lead-free double perovskites," Light: Sci. Appl. **11**, 52 (2022).
[70] M. B. Gray, J. D. Majher, T. A. Strom, and P. M. Woodward, "Broadband white emission in $Cs_2AgIn_{1-x}Bi_xCl_6$ phosphors," Inorg. Chem. **58**, 13403–13410 (2019).
[71] M. Jeevaraj, P. Devendran, N. Nallamuthu, S. Sudhahar, and M. K. Kumar, "Influence of Mn^{2+} doping on the optical properties of $Cs_2AgBiCl_6$ double perovskite luminescent phosphors," J. Mater. Sci.: Mater. Electron. **34**, 65 (2023).
[72] F. Ji *et al.*, "The atomic-level structure of bandgap engineered double perovskite alloys $Cs_2AgIn_{1-x}Fe_xCl_6$," Chem. Sci. **12**, 1730–1735 (2021).
[73] H. Yin *et al.*, "An emerging lead-free double-perovskite $Cs_2AgFeCl_6$: In single crystal," Adv. Funct. Mater. **30**, 2002225 (2020).
[74] H. Lei, D. Hardy, and F. Gao, "Lead-free double perovskite $Cs_2AgBiBr_6$: Fundamentals, applications, and perspectives," Adv. Funct. Mater. **31**, 2105898 (2021).
[75] E. Greul, M. L. Petrus, A. Binek, P. Docampo, and T. Bein, "Highly stable, phase pure $Cs_2AgBiBr_6$ double perovskite thin films for optoelectronic applications," J. Mater. Chem. A **5**, 19972–19981 (2017).
[76] W. Tress and M. T. Sirtl, "$Cs_2AgBiBr_6$ double perovskites as lead-free alternatives for perovskite solar cells?," Sol. RRL **6**, 2100770 (2022).
[77] K. P. Lindquist *et al.*, "Tuning the bandgap of $Cs_2AgBiBr_6$ through dilute tin alloying," Chem. Sci. **10**, 10620–10628 (2019).
[78] F. Ji *et al.*, "Lead-free halide double perovskite $Cs_2AgBiBr_6$ with decreased band gap," Angew. Chem. **132**, 15303–15306 (2020).
[79] F. Ji *et al.*, "Near-infrared light-responsive Cu-doped $Cs_2AgBiBr_6$," Adv. Funct. Mater. **30**, 2005521 (2020).
[80] Z. Zhang *et al.*, "Hydrogenated $Cs_2AgBiBr_6$ for significantly improved efficiency of lead-free inorganic double perovskite solar cell," Nat. Commun. **13**, 3397 (2022).
[81] W. Ning *et al.*, "Magnetizing lead-free halide double perovskites," Sci. Adv. **6**, eabb5381 (2020).
[82] G. Liu *et al.*, "Extending absorption of $Cs_2AgBiBr_6$ to near-infrared region (≈1350 nm) with intermediate band," Adv. Funct. Mater. **32**, 2109891 (2022).
[83] M. N. Tran, I. J. Cleveland, J. R. Geniesse, and E. S. Aydil, "High photoluminescence quantum yield near-infrared emission from a lead-free ytterbium-doped double perovskite," Mater. Horiz. **9**, 2191–2197 (2022).
[84] M. N. Tran, I. J. Cleveland, and E. S. Aydil, "Reactive physical vapor deposition of Yb-doped lead-free double perovskite $Cs_2AgBiBr_6$ with 95% photoluminescence quantum yield," ACS Appl. Electron. Mater. **4**, 4588–4594 (2022).
[85] O. Stroyuk *et al.*, "Highly luminescent transparent $Cs_2Ag_xNa_{1-x}Bi_yIn_{1-y}Cl_6$ perovskite films produced by single-source vacuum deposition," ACS Mater. Lett. **5**, 596–602 (2023).